ENDOR Spectroscopic Evidence for the Position and Structure of N^G-Hydroxy-L-arginine Bound to Holo-Neuronal Nitric Oxide Synthase†

David L. Tierney, Hui Huang, Pavel Martasek, Bettie Sue Siler Masters,* Richard B. Silverman,* and Brian M. Hoffman*

Department of Chemistry and Department of Biochemistry, Molecular Biology, and Cell Biology, Northwestern University, Evanston, Illinois 60208-3113, and Department of Biochemistry, The University of Texas Health Science Center, San Antonio, Texas 78284-7760

Received December 9, 1998; Revised Manuscript Received January 27, 1999

ABSTRACT: Recently, we used 35 GHz pulsed ^{15}N ENDOR spectroscopy to determine the position of the reactive guanidino nitrogen of substrate L-arginine relative to the high-spin ferriheme iron of holo-neuronal nitric oxide synthase (nNOS) [Tierney, D. L., et al. (1998) *J. Am. Chem. Soc. 120*, 2983−2984]. Analogous studies of the enzyme-bound reaction intermediate, N^G-hydroxy-L-arginine (NOHA), singly labeled with ^{15}N at the hydroxylated nitrogen (denoted N_R), show that N_R is held 3.8 Å from the Fe, closer than the corresponding guanidino N of L-Arg (4.05 Å). ^{1,2}H ENDOR of NOHA bound to holo-nNOS in H_2O and D_2O discloses the presence of a single resolved exchangeable proton (H1) 4.8 Å from Fe and very near the heme normal. The ENDOR data indicate that NOHA does not bind as the resonance-stabilized cation in which the terminal nitrogens share a positive charge. ENDOR-determined structural constraints permit two alternate structural models for the interaction of NOHA with the high-spin heme iron. In one model, H1 is assigned to the O-H proton; in the other, it is the N_R-H proton. However, the alternatives differ in the placement of the N−O bond relative to the heme iron. Thus, a combination of the ENDOR data with appropriate diffraction studies can achieve a definitive determination of the protonation state of N_R and thus of the tautomeric form that is present in the enzyme−NOHA complex. The mechanistic implications of this result are further discussed.

Nitric oxide synthase (EC 1.14.13.39, NOS) is reponsible for the in vivo generation of nitric oxide, an important hormone and neurotransmitter that regulates a variety of physiological functions (*1*). NOS exists in at least three isozymic forms: one in endothelial cells (eNOS), which regulates smooth muscle relaxation and, therefore, blood pressure; one in neuronal cells (nNOS), involved in brain development and memory; and an inducible form in macrophage cells (iNOS), produced during an immune response. All of the isozymes require multiple cofactors in three binding domains. The N-terminal domain, or oxygenase domain, binds heme and tetrahydrobiopterin (as well as the substrate); the C-terminal domain, or reductase domain, binds NADPH, FAD, and FMN (*2*), and connecting these two domains is a third domain which binds calcium and/or calmodulin and may act as an intermediary to electron transfer between the reductase and oxygenase domains (*3*).

The reaction catalyzed by NOS is the conversion of L-arginine (**1**) to L-citrulline (**2**) and nitric oxide (Scheme 1). The initial step in this conversion is N-hydroxylation of the guanidine group of L-arginine to give N^G-hydroxy-L-arginine (NOHA) (*4*). The nitrogen atom of nitric oxide is derived from the guanidine nitrogen of L-arginine (*5*) and from the nitrogen to which the hydroxyl group of NOHA is attached (*4*, *6*). The oxygen atoms of both nitric oxide and the carbonyl of citrulline come from two separate molecules of dioxygen (*7*, *8*).

Various reasonable mechanisms have been proposed for the conversion of L-arginine to L-citrulline and nitric oxide via NOHA (*9*−*13*). However, there appears to be no agreement about the structure of the bound intermediate. Most research groups (*11*, *12*, *14*−*22*) prefer to depict NOHA as structure **3** (Scheme 2), but some use structure **4** (*23*, *24*) and others structure **5** (*25*, *26*). The main reason for this apparent inconsistency is that there is no evidence for the geometry and protonation state of this intermediate when it is bound to nitric oxide synthase, and therefore, all of these structures are reasonable.

Recently, as part of a larger effort to extend the use of ENDOR of metalloenzymes for obtaining geometric information about atoms beyond the coordination sphere of the metal ion, we used 35 GHz Mims pulsed ENDOR spectroscopy to elucidate the geometry of ^{15}N-labeled L-arginine bound to the nNOS holoenzyme (*27*). In that report, the dipolar hyperfine coupling, measured over a limited range of fields near $g_2 = 4.19$, was used to deduce a heme iron-to-guanidino nitrogen distance of 4.05 Å, which has been beautifully confirmed in X-ray diffraction studies of the heme domains of eNOS (*28*), nNOS (*29*), and iNOS (*17*). We now extend the use of this methodology to examine the structure of the reaction intermediate NOHA bound to holo-nNOS, in particular addressing the question of whether the hy-

† We are grateful to the National Institutes of Health [to B.M.H. (HL13531), to D.L.T. (GM18432), to R.B.S. (GM49725), and to B.S.S.M. (GM52419)] and the Robert A. Welch Foundation [to B.S.S.M. (AQ-1192)] for financial support of this research.

10.1021/bi982904r CCC: $18.00
Published on Web 03/05/1999

Scheme 1

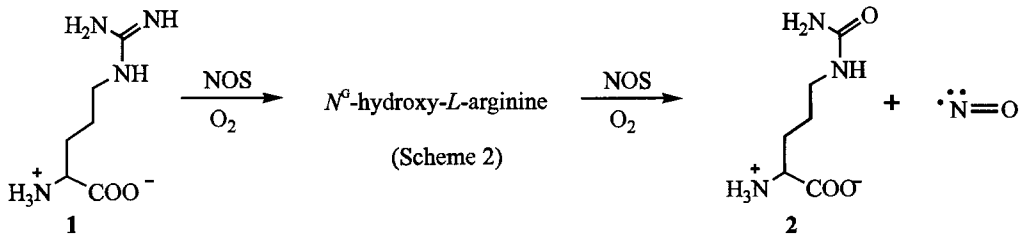

Scheme 2

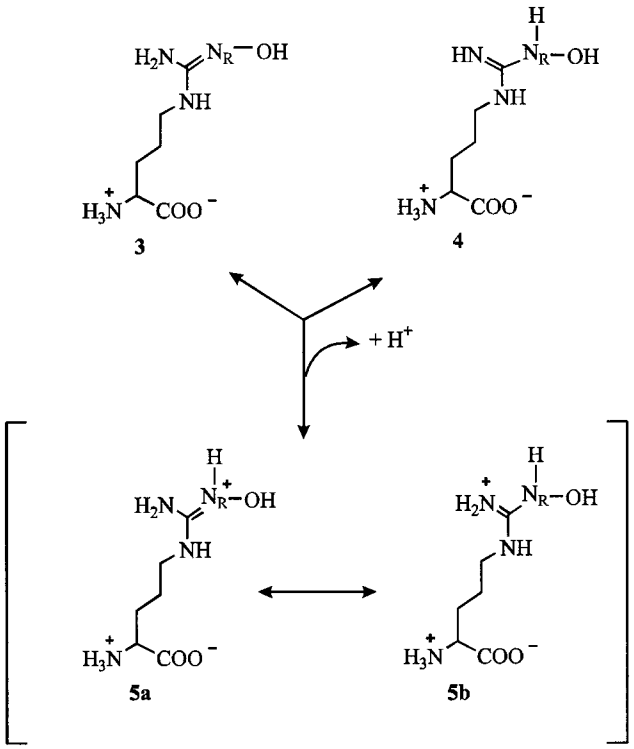

droxylated nitrogen of NOHA bears an N-H proton, as in **4** and **5**, or does not, as in **3**.

MATERIALS AND METHODS

The purified nNOS holoenzyme was prepared as described previously (*30*). NOHA labeled with ^{15}N at the hydroxylated nitrogen was prepared from L-citrulline and $^{15}NH_2OH$ according to published procedures (*31*). ENDOR samples were prepared by twice diluting 60 μL of 0.5 mM nNOS to 600 μL with 5 mM NOHA in either D_2O or H_2O buffer and incubating for 24 h at 4 °C before concentrating back to 60 μL (*27*).

ENDOR spectra were recorded on instruments of local design and construction in either the CW (*32*) or pulsed (*33*) mode. Proton H−D difference spectra were obtained by subtraction of absolute pulsed ENDOR spectra of samples prepared in H_2O and D_2O buffers, following the procedure described by Doan et al. (*34*). Two independently prepared samples were measured in each solvent.

The ENDOR spectra were interpreted using an idealized dipolar model (*35*), in which the intrinsic dipolar interaction between the high-spin ferric ion ($S = {}^5/_2$) and a nucleus has the form $\mathbf{T} = [-T, -T, 2T]$, where $T = \rho_{Fe} g_e g_N \beta_e \beta_N / r^3$, in a coordinate frame where the unique direction corresponds to the iron−nucleus vector. The nuclear and electronic g factors (g_N and g_e, respectively) and the electronic and nuclear magnetons (β_e and β_N, respectively) take their known values; r is the distance from the nucleus to the heme iron, and ρ_{Fe} is the effective fraction of the electron spin on the iron. An appropriate choice for this parameter accommodates the fact that, for simplicity, interactions with the remainder of the spin on the pyrrole nitrogens, etc., are not included explicitly. This choice for ρ_{Fe} is supported by a crystallographic determination of an Fe···N_g distance of 4.07 Å for L-Arg bound to nNOS (*29*), as compared to the value of 4.05 Å calculated from ENDOR data using $\rho_{Fe} = 0.9$. While such agreement is better than the joint precision of the measurements, because the distance estimate varies as $\rho_{Fe}^{1/3}$, a modest variation in this parameter is expected to contribute little to the uncertainty in r.

For a given molecular orientation relative to the external field, the interaction of the ferric ion with a nonligand nucleus with a spin I of ${}^1/_2$ (e.g., ^1H and ^{15}N) gives a doublet whose hyperfine splitting (denoted A) is determined by T; for the ^2H ($I = 1$) nucleus, each line of the doublet is further split by the quadrupole interaction. The strong **g** anisotropy of the nNOS ferriheme modifies the intrinsic hyperfine interaction, scaling the observed hyperfine coupling. For example if the Fe−nuclear vector were parallel to g_3, the effective coupling would be rhombic: $\mathbf{T}' = [T_1', T_2', T_3'] = [-(g_1/g_e)T, -(g_2/g_e)T, 2(g_3/g_e)T]$; the noncoaxiality of **g** and **T** alters this result. Procedures have been devised for determining hyperfine matrices through analysis of a two-dimensional set of ENDOR spectra taken at fields across the EPR envelope (*36*), but for dipolar interactions, less extensive data sets can suffice (*27*). For example, simulations show that no matter what the actual orientation of the Fe−nuclear vector, the doublet splitting in ENDOR spectra taken near g_2 for a frozen solution depends only on the Fe−nuclear distance (it is roughly equal to T_2'), while the line shapes are fixed by the orientation of the vector relative to the heme.

To model the location of NOHA bound near the nNOS ferriheme, the software package Chem Office (ChemDraw and CHEM3D, CambridgeSoft Corp., Cambridge, MA) was used to construct and position the intermediate subject to normal geometric constraints supplemented by ENDOR-derived ones (Figure 2). Each of the structures (**3**−**5**) was drawn in ChemDraw and imported into CHEM3D. Each of these structures naturally folded into an "L" shape when imported into CHEM3D, and retained this configuration and appropriate internuclear distances after energy minimization. As we are able to probe only the hydroxyguanidine end of NOHA, and did not attempt to accommodate the rest of the molecule within the heme pocket, the overall shapes of **3**−**5** were left unaltered.

Each structure was then placed above a model of the heme, with analogy to L-Arg binding. Although crystallographic

coordinates are not yet available for the binding of L-Arg to the iNOS heme domain, examination of the published structure (*17*) reveals that L-Arg binds to the enzyme with the guanidino moiety held in a planar conformation lying roughly parallel to and directly above the heme plane, very nearly in van der Waals contact with the porphyrin. Each of the structures (**3**−**5**) contains a hydroxyguanidine moiety with a trigonal-planar central carbon atom, which also requires that the four "heavy" atoms (imine N, central C, amine N, and hydroxy N_R) lie in a plane, as with L-Arg.

The $^{15}N_R$ data allow for a precise determination of the position of N_R; the $^{1,2}H$ data provide a less precise, independent location for an exchangeable NOHA proton, H1 (see below). Therefore, the first ENDOR constraint was applied to the placement of N_R. On the basis of a close approach of N_R to the heme iron, we began with an idealized placement of the planar portion of the side chain roughly parallel to the heme and near to van der Waals contact. After a permissible position of N_R was chosen, constraints on the location of exchangeable protons were applied. We then explored rotations and translations of the hydroxyguanidino fragment in the plane parallel to the heme, with little tilt relative to the heme plane. Single bonds were allowed to experience free rotation where appropriate, so all possible arrangements that would simultaneously satisfy the ^1H and ^{15}N ENDOR constraints could be explored. In structure **4** for example, where N_R is pyramidal, placement of the protons introduces two extra degrees of freedom: (1) rotation about the C−N_R bond, which changes the placement of both the N_R-H and O-H protons, and (2) rotation about the N_R−O bond, which adjusts the position of the hydroxyl proton only. For structure **3** and the resonance-stabilized cation **5**, where N_R is trigonal planar, only the rotation about the N_R−O bond adds a degree of freedom.

To test a given arrangement, the distance to each exchangeable proton of NOHA was calculated. The angles θ, defined as the angle between the Fe−H vector and the normal to the heme passing through Fe (g_z axis), and ϕ, the angle between the Fe−$N_{pyrrole}$ bonds and the projection of the Fe−H vector onto the heme plane, were estimated on the basis of the proton's position. For each exchangeable proton, the three parameters were used to generate theoretical ENDOR spectra, and the simulations for all the exchangeable protons were then summed and the resultant spectra compared to experiment. Systematic variation of the angular parameters shows that the ENDOR intensity at g_1 for a proton interacting with a high-spin ferriheme decreases rapidly with increasing θ, becoming nearly unobservable when $\theta \geq 10°$ (Figure 3B). Consequently, among models that satisfy the ^{15}N constraints, only positions for proton H1 within ∼10−15° of the heme normal were considered acceptable. We note that for such a small value of θ, variations in ϕ have little effect.

RESULTS

EPR. EPR spectra for holo-nNOS with NOHA bound (not shown) disclose a high-spin ferriheme with the following g values: [g_1, g_2, g_3] = [7.65, 4.03, ∼1.8], where g_3 corresponds to the heme normal. These differ little from those of the enzyme with the substrate L-Arg bound, indicating that the Fe remains five-coordinate with bound NOHA, as it is

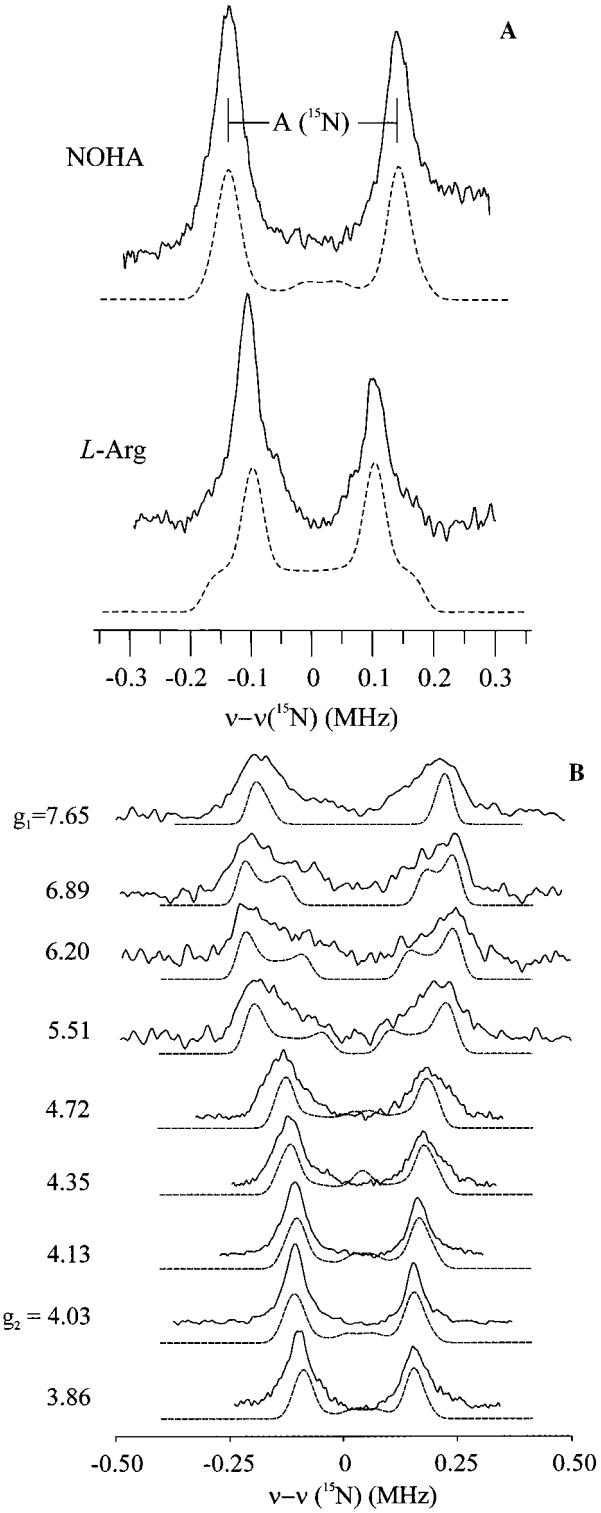

FIGURE 1: (A) ^{15}N 35 GHz Mims pulsed ENDOR spectra taken at g_2 for holo-nNOS with bound [^{15}N]-N^G-hydroxy-L-arginine (g_2 = 4.03, top) and with bound [$^{15}N_g$]-L-arginine (g_2 = 4.19, bottom). The conditions were as follows: T = 2 K, ν_{MW} = 34.70 GHz, MW pulse lengths of 40 ns, τ = 800 ns, RF pulse length of 40 μs, and a repetition rate of 200 Hz. Each spectrum consists of 256 points, with each point an average of 6000 transients. The dotted lines are simulations based on an Fe···N distance of 3.8 Å, with Euler angles of θ = 10° and ϕ = 45° for NOHA, and with an Fe···N distance of 4.05 Å and θ = 15° and ϕ = 45° for L-Arg. (B) Field-dependent data for nNOS with bound [$^{15}N_R$]NOHA. The conditions for data collection were as described for panel A. The simulations (dotted lines) include 15 kHz of isotropic coupling, and the r, θ, and ϕ parameters were adjusted manually to match the splittings in the experimental data.

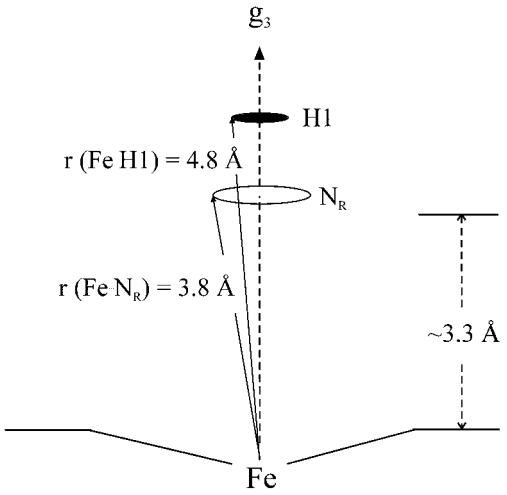

FIGURE 2: Structural constraints based on the ENDOR data. The hydroxylated nitrogen, N_R, lies on the circle 3.8 Å from Fe (θ = 10°); H1 is confined to lie within the circle at 4.8 Å ($\theta \leq 5°$). The vertical bar on the right represents the combined van der Waals thickness of the heme and N_R.

with bound L-Arg (*37*). Despite the fact that hydroxamates are well-known ferric ion ligands, the intermediate only weakly perturbs the heme iron, but does not coordinate to it.

ENDOR. Figure 1A presents Mims pulsed ^{15}N ENDOR spectra for holo-nNOS in the presence of NOHA singly labeled with ^{15}N at the hydroxylated nitrogen (denoted N_R in Scheme 2), and in the presence of [$^{15}N_g$]-L-Arg. The spectra are similar in shape, but the doublet splitting at g_2, which is a direct measure of the heme Fe-to-^{15}N distance (*27*, *38*), is notably greater for NOHA [$A(^{15}N)$ = 0.28 MHz] than it is for L-Arg [$A(^{15}N)$ = 0.22 MHz]. Analysis of the data gives an r(Fe···$^{15}N_R$) of 3.80 Å for NOHA, significantly shorter than that for the corresponding guanidino nitrogen of L-Arg (4.05 Å). To refine the geometric parameters, a two-dimensional set of ^{15}N spectra was recorded for NOHA-bound nNOS at fields from g_1 = 7.65 to just above g_2. At higher fields, the EPR signals of the high-spin, substrate-bound and low-spin, substrate-free species overlap and reliable ENDOR data could not be obtained. Simulations of the two-dimensional pattern indicate that N_R is held more nearly over the iron (~10° off the heme normal, Figure 2) than the guanidino nitrogen of L-Arg (~15° off normal)[1] and lies roughly over a line in the heme plane that falls between the Fe−$N_{pyrrole}$ bonds.[2]

Each of the structures (**3**−**5**) contains several distinct labile protons in the vicinity of N_R (four in structures **3** and **4** and five in structure **5**). The close proximity of the $^{15}N_R$ of NOHA to the heme iron requires that all of these protons fall within ~6 Å of the iron. To probe the exchangeable protons, we have employed 35 GHz pulsed $^{1,2}H$ ENDOR, using a modified version of the Mims technique, the refocused Mims (Re-Mims) protocol (*39*). A comparison of the Re-Mims proton ENDOR spectra for NOHA bound to nNOS in H_2O and D_2O at g_1 = 7.65 (Figure 3) discloses the presence of an exchangeable proton (H1) with a dipolar coupling A_1 of 2.5 MHz. This is most clearly visualized in the H_2O-D_2O difference spectrum, and is corroborated by the ^2H spectrum whose breadth is comparable to that of the proton; the slightly larger width of the ^2H spectrum is due to the ^2H quadrupole interaction. Simulations of the ^1H spectrum at g_1, shown in Figure 3, and of others taken over a range of fields (data

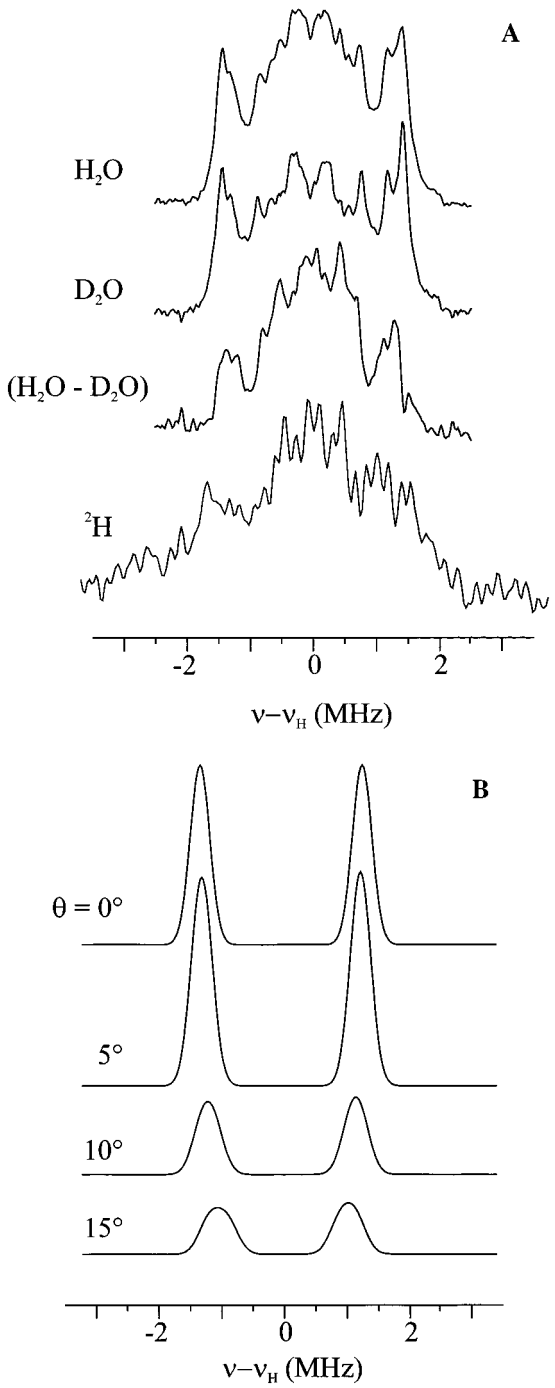

FIGURE 3: (A) 35 GHz Re-Mims ^1H and Mims ^2H ENDOR spectra taken at g_1 = 7.65 for NOHA bound to holo-nNOS. The *x*-axis of the ^2H spectrum has been scaled by a factor of 6.58 (g_H/g_D). The conditions were as follows: T = 2 K, τ = 140 ns for ^1H and 600 ns for ^2H, MW pulse lengths of 28, 28, 28, and 60 ns, and 3000 transients; other conditions were as described in the legend of Figure 1. (B) Theoretical ^1H ENDOR spectra at g_1 = 7.65 for a dipolar interaction between the high-spin ferriheme of nNOS and a proton at 4.8 Å and different values of θ.

[1] The increased angular precision afforded by a larger range of available fields has led to a redetermination of the angles (θ = 15° and ϕ = 45°) for [$^{15}N_g$]-L-Arg bound to nNOS, compared to the earlier estimates of 10° and 15°, respectively.

[2] Continuous-wave ENDOR of the pyrrole nitrogens at 35 GHz (not shown) gives a pair of well-resolved two-line patterns at g_1 and g_2 indicating that g_x and g_y lie along the Fe−$N_{pyrrole}$ bonds.

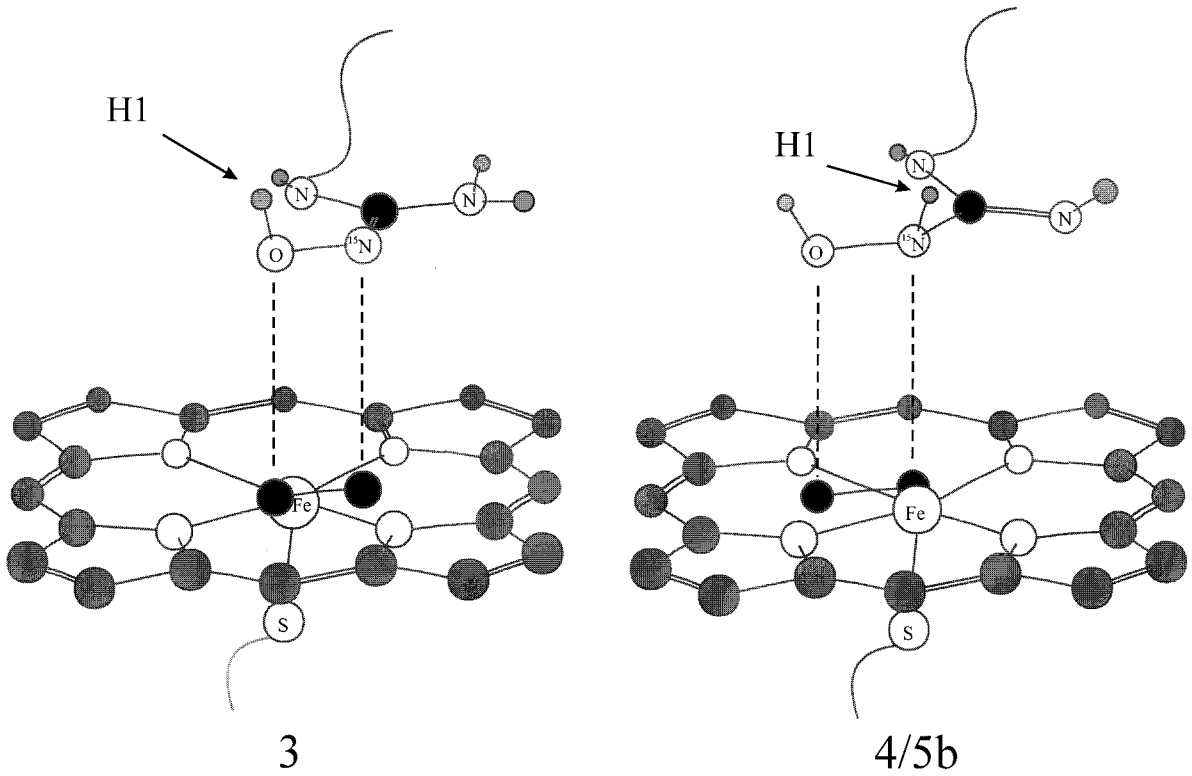

FIGURE 4: Three-dimensional models of NOHA bound to nNOS based on the ENDOR-derived constraints. The protons of NOHA, as well as the carbons of the porphyrin, are gray; the pyrrole nitrogens are white, and the central carbon of NOHA is black. For the purpose of comparison, the N−O bond of NOHA is projected in black onto the heme plane: **(**left**)** structure **3** in Scheme 2 and (right**)** structures **4** and **5b** in Scheme 2.

not shown), indicate that the sharp H1 signals must be assigned to a proton that resides ca. 4.8 Å from the heme iron and within ∼5−10° of the heme normal (Figure 2). Packing constraints require that this H1 signal come from a single proton. The g_1 difference spectrum shows no intensity from another nearby exchangeable proton with ^{1}H hyperfine couplings of >2 MHz. Data taken at other fields show no intensity, other than that of H1, that could arise from such a proton. This indicates that none of the other protons on NOHA is closer than ∼5.3 Å.

Analysis. For the range of ENDOR-permitted positions of N_R, most placements of the terminal, planar four-atom fragment of the hydroxyguanidino moiety require the assignment of H1 to a proton associated with the [N_R-OH] (**3**) or [N_R(H)-OH] (**4** and **5**) moiety. For **4** and **5**, an assignment of H1 to a proton on the remote terminal nitrogen would require the proton to be almost 1 Å too close to the heme. As described in Materials and Methods, we explored the allowed placements of NOHA with respect to the heme for **3** and for each of the two possible assignments of the proton resonance for **4** and **5** [[N_R(H1)-OH] and [N_R(H)-OH1]].

Within the constraints, it is not possible to build a model in which H1 corresponds to either the N_R-H proton or the O-H proton attached to the trigonal-planar N_R of the resonance-stabilized cationic form of NOHA, **5**. In this case, either assignment as H1 must place the other proton too close to the Fe ion to be compatible with the absence of a second exchangeable proton with a hyperfine coupling of >2 MHz. Hence, we conclude that enzyme-bound NOHA does not exist as such a resonance-stabilized cation.

If, however, the conjugation of **5** is broken by rotation about the C−N_R bond, leading to pyramidalization of N_R, then **5** no longer has two resonance forms; it is better represented as a single structure (namely, **5b**) in which the geometry of N_R is similar to that of **4**. Therefore, for further modeling we treated **4** and **5** as equivalent, since the only difference between these two in the absence of resonance would be the protonation state of the remote sp^2 nitrogen atom. It is not possible to build a model in which H1 corresponds to the O-H proton of **4** or **5**. Any such model places the N_R-H proton at a distance of 3.7 Å and very near the heme normal, in which case at fields near g_1 it must give a sharp, exchangeable proton signal with an $A(^1H)$ of >5 MHz. However, no such signal exists.

It is possible to build a model in which H1 corresponds to the OH proton of structure **3**, and likewise for the N_R-H proton of **4** or **5**; Figure 4 illustrates the best models for **3** and **4**. Both of these models satisfy the ENDOR constraints, placing the $^{15}N_R$ at the proper distance (3.8 Å) and offset from the heme normal (∼10°), and placing a single exchangeable proton nearly along the g_z axis. However, because the models differ in the identity of proton H1, they differ in the placement of the N−O bond above the heme. This is illustrated by the projection of the N−O bond onto the heme plane, shown in Figure 4. For **4** and **5** (Figure 4, right), where the H1 signal is assigned to the N_R-H proton of a pyramidal R-NHOH fragment, the N of the N−O bond lies roughly over the Fe, with the hydroxyl proton at too great a distance to give a hyperfine coupling of ≥2 MHz, as required. For **3** (Figure 4, left), where H1 is the hydroxyl proton, the O of the N−O bond is almost directly above the iron, with the hydroxyl proton extending upward, to form an N−O−H "cap". A second model for **3**, in which H1 is assigned as an amine proton on the other terminal nitrogen, also satisfies

the ENDOR requirements (not shown). However, this model extends the N_R-O bond away from the iron and places the hydroxyl proton at a considerable distance from Fe, whereas mechanistic studies suggest that the first step in the reduction of NOHA is abstraction of the hydroxyl hydrogen atom by an iron-bound oxygen species.

Looked at from the side, both models in Figure 4 have the five side chain atoms (amine N, imine N, *N*-hydroxy N, central C, and hydroxyl O) lying roughly in a plane parallel to that of the heme. This geometry is required for **3**, while it emerges from the ENDOR-derived constraints when modeling the binding of **4** and **5**. Nonetheless, the ENDOR-determined constraints do not distinguish between the two possibilities.

DISCUSSION

Pulsed ^{15}N ENDOR measurements have disclosed that the reactive nitrogen of NOHA, N_R, lies near to and almost directly above the heme iron of ferric holo-nNOS (Figure 2), even closer than the reactive guanidino N of L-Arg. The $^{1,2}H$ ENDOR data indicate that NOHA does not bind to nNOS as the resonance-stabilized cation, **5**, in which the terminal nitrogens share a positive charge. The data permit three alternate assignments for the most strongly coupled exchangeable proton; two of these involve **3**, one with H1 as the O-H proton as seen in the left panel of Figure 4 and one as an H on the other terminal N (not shown), and the third is as the N_R-H proton of **4** and **5b** in the right panel of Figure 4. All three models fix the N−O bond in a plane parallel to that of the heme. However, these alternatives differ in the placement of the N−O bond relative to the heme iron.

The protonation state of N_R thus can be determined by combining the current ENDOR data with the results of an appropriate X-ray diffraction study of the NOHA-bound enzyme. Although diffraction cannot locate the proton(s) directly, it can determine which idealized structure derived from the ENDOR constraints has an N−O bond position corresponding to that of either **3** or **4**/**5b** in Figure 4. Thus, the two techniques together will permit a definitive determination of the protonation state of the reactive N_R of enzyme-bound N^G-hydroxy-L-arginine, and of the tautomer that binds to the enzyme.

The protonation state and tautomeric form of NOHA should have a significant bearing on the function of nitric oxide synthase. In a commonly drawn mechanism, the conversion of NOHA to L-citrulline and NO is initiated by hydrogen atom abstraction from the hydroxyl group of NOHA, leaving an oxy radical on the substrate (*15*−*17*, *20*). Examination of all possible resonance forms for an oxy radical derived from forms **3**−**5** suggests that the ease of hydrogen atom abstraction would follow the order **3** > **4** > **5**. The ENDOR-derived conclusion that **5** does not represent the form of bound NOHA is thus consistent with this mechanism. Indeed, the mechanism suggests that bound NOHA should be described by structure **3**.

NOTE ADDED IN PROOF

Since the acceptance of this paper, we have learned that Drs. C. S. Raman and Huiying Li and Prof. T. L. Poulos have determined the X-ray crystal structure of the heme domain of nNOS with NOHA bound. They find that the position of NOHA, and in particular of the NO bond, corresponds to our structure **4**/**5b** in Figure 4. Thus, the two techniques together show that the bound form of NOHA *is not* **3**, but rather *is* **4**/**5b**, with an [-N_RH(OH)] fragment. This appears to be noteworthy, given that the current mechanism would favor **3**, and that the positioning of NOHA does not seem to place the hydroxyl H in a favorable position for the proposed abstraction by a high-valence reaction intermediate.

ACKNOWLEDGMENT

We thank Prof. Paul Ortiz de Montellano for stimulating discussion.

REFERENCES

1. Masters, B. S. S., Martasek, P., and Roman, L. J. (1998) *The Physiology and Clinical Applications of Nitric Oxide* (Rubanyi, G. M., Ed.) Gordon and Breach Publishing Group, London.
2. Masters, B. S. S., McMillan, K., Sheta, E. A., Nishimura, J. S., Roman, L. J., and Martasek, P. (1996) *FASEB J. 10*, 552.
3. Abu-Soud, H. M., Yoho, L. L., and Stuehr, D. J. (1994) *J. Biol. Chem. 269*, 32047.
4. Stuehr, D. J., Kwon, N. S., Nathan, C. F., Griffith, O. W., Feldman, P. L., and Wiseman, J. (1991) *J. Biol. Chem. 266*, 6259.
5. Tayeh, M. A., and Marletta, M. A. (1989) *J. Biol. Chem. 264*, 19654.
6. Pufahl, R. A., Nanjappan, P. G., Woodard, R. W., and Marletta, M. A. (1992) *Biochemistry 31*, 6822.
7. Kwon, N. S., Nathan, C. F., Gilker, C., Griffith, O. W., Matthews, D. E., and Stuehr, D. J. (1990) *J. Biol. Chem. 265*, 13442.
8. Leone, A. M., Palmer, R. M. J., Knowles, R. G., Francis, P. L., Ashton, D. S., and Moncada, S. (1991) *J. Biol. Chem. 266*, 23790.
9. Stuehr, D. J., and Griffith, O. W. (1992) *Adv. Enzymol. 65*, 287.
10. Marletta, M. A. (1993) *J. Biol. Chem. 268*, 12231.
11. Korth, H. G., Sustmann, R., Thater, C. C., Butler, A. R., and Ingold, K. U. (1994) *J. Biol. Chem. 269*, 17776.
12. Kerwin, J. F., Lancaster, J. R., and Feldman, P. L. (1995) *J. Med. Chem. 38*, 4342.
13. Pufahl, R. A., Wishnok, J. S., and Marletta, M. A. (1995) *Biochemistry 34*, 1930.
14. Masters, B. S. S. (1994) *Annu. Rev. Nutr. 14*, 131.
15. Rusche, K. M., Spiering, M. M., and Marletta, M. A. (1998) *Biochemistry 37*, 15503.
16. Clague, M. A., Wishnok, J. S., and Marletta, M. A. (1997) *Biochemistry 36*, 14465.
17. Crane, B. R., Arvai, A. S., Ghosh, D. K., Wu, C., Getzoff, E. D., Stuehr, D. J., and Tainer, J. A. (1998) *Science 279*, 2121.
18. Abu-Soud, H. M., Presta, A., Mayer, B., and Stuehr, D. J. (1997) *Biochemistry 36*, 10811.
19. Wang, J., Stuehr, D. J., and Rousseau, D. L. (1997) *Biochemistry 36*, 4595.
20. Fukuto, J. M., Stuehr, D. J., Feldman, P. L., Bova, M. P., and Wong, P. (1993) *J. Med. Chem. 36*, 2666.
21. Klatt, P., Schmidt, K., Uray, G., and Mayer, B. (1993) *J. Biol. Chem. 268*, 14781.
22. Renaud, J. P., Boucher, J. L., Vadon, S., Delaforge, M., and Mansuy, D. (1993) *Biochem. Biophys. Res. Commun. 192*, 53.
23. Zhang, H. Q., Dixon, R. P., Marletta, M. A., Nikolic, D., Breemen, R. V., and Silverman, R. B. (1997) *J. Am. Chem. Soc. 119*, 10888.
24. DeMaster, E. G., Raij, L., Archer, S. L., and Weir, E. K. (1989) *Biochem. Biophys. Res. Commun. 163*, 527.
25. Olken, N. M., and Marletta, M. A. (1992) *J. Med. Chem. 35*, 1137.
26. Feldman, P. L., Griffith, O. W., Hong, H., and Stuehr, D. J. (1993) *J. Med. Chem. 36*, 491.
27. Tierney, D. L., Martasek, P., Doan, P. E., Masters, B. S. S., and Hoffman, B. M. (1998) *J. Am. Chem. Soc. 120*, 2983.

28. Raman, C. S., Li, H., Martasek, P., Kral, V., Masters, B. S. S., and Poulos, T. L. (1998) *Cell* (in press).
29. Raman, C. S., Poulos, T. L., Li, H., Martasek, P., and Masters, B. S. S. (1998) Unpublished results.
30. Roman, L. J., Sheta, E. A., Martasek, P., Gross, S. S., Liu, Q., and Masters, B. S. S. (1995) *Proc. Natl. Acad. Sci. U.S.A. 92*, 8428.
31. Wagenaar, F. L., and Kerwin, J. F. (1993) *J. Org. Chem. 58*, 4331.
32. Werst, M. W., Davoust, C. E., and Hoffman, B. M. (1991) *J. Am. Chem. Soc. 113*, 1533.
33. Davoust, C. E., Doan, P. E., and Hoffman, B. M. (1996) *J. Magn. Reson. A119*, 38.
34. Doan, P. E., Fan, C., and Hoffman, B. M. (1994) *J. Am. Chem. Soc. 116*, 1033.
35. Hutchison, C. A., and McKay, D. B. (1977) *J. Chem. Phys. 66*, 3311.
36. Hoffman, B. M., DeRose, V. J., Doan, P. E., Gurbiel, R. J., Houseman, A. L. P., and Telser, J. (1993) *Biological Magnetic Resonance* (Berliner, L. J., and Reuben, J., Eds.) Plenum Press, New York.
37. Salerno, J. C., McMillan, K., and Masters, B. S. S. (1996) *Biochemistry 35*, 11839.
38. Mustafi, D., Knock, M. M., Shaw, R. W., and Makinen, M. W. (1997) *J. Am. Chem. Soc. 119*, 12619.
39. Doan, P. E., and Hoffman, B. M. (1997) *Chem. Phys. Lett. 269*, 208.

BI982904R